First publ. in: Journal of Applied Physics 88 (2000), 7, pp. 4221-4225

Micromagnetism and high temperature coercivity of MnBi/Al multilayers

U. Rüdiger[a)] and G. Güntherodt
RWTH Aachen, 2. Physikalisches Institut, D-52056 Aachen, Germany

P. Fumagalli
FU Berlin, Institut für Experimentalphysik, Arnimallee 14, D-14195 Berlin, Germany

L. Thomas and S. S. P. Parkin
IBM Research Division, Almaden Research Center, San Jose, California 95120

A. D. Kent
Department of Physics, New York University, New York, New York 10003

(Received 18 April 2000; accepted for publication 5 July 2000)

The micromagnetic properties of multilayered MnBi/Al films have been investigated and compared to pure MnBi thin films. Pure MnBi films reveal an anomalous increase of the high temperature coercivity, which has been explained on the basis of a hybrid domain wall pinning model. The multilayer-type preparation of MnBi/Al thin films results in significantly reduced MnBi particle size of approximately 40 nm. The smaller particle size leads to a change of the dominant magnetization reversal process from one driven by domain wall movement toward coherent rotation. This was investigated via magnetic force microscopy imaging and micromagnetic calculations. The absence of domain walls during magnetization reversal results in a clear suppression of the increase of the high temperature coercivity observed in pure MnBi films.

I. INTRODUCTION

The ferromagnetic compound MnBi has been considered as a promising candidate for a magneto-optical (MO) recording medium for more than 40 yr.[1–4] The most striking features in the polar Kerr rotation spectrum of MnBi are two maxima of approximately 1.0° at $h\nu = 1.8$ eV and $h\nu = 3.6$ eV,[5,6] respectively. This results at a higher photon energy range in a larger figure-of-merit than observed in Co/Pt multilayers and amorphous TbFeCo thin films.[7] The first maximum at 1.8 eV is related to interband transitions of electrons from occupied Bi($6p$) states to unoccupied Mn($3d$) states.[8–10] The peak at 3.6 eV seems to correspond to partially oxidized MnBi, which leads to interband transitions from occupied O($2p$) states to unoccupied Mn($3d$) states.[6,8,11] This observation is in contrast to previous calculations, where the second maximum in the range of 3.4 eV has been interpreted as an interband transition from occupied Mn($3d$) states to unoccupied Bi($6p$) states.[9,10] Variations of the Mn–Bi stoichiometry have been also discussed as the origin for the large experimentally determined polar Kerr rotation in the same spectral region, which is not consistent with first principles band structure calculations of pure MnBi.[12] Systematic studies on Al-doped thin films as well as band structure calculations show that a small amount of Al does not significantly affect the polar Kerr rotation spectrum.[4,9]

After the successful development of the blue GaN laser diode ($\lambda = 417$ nm) the large polar Kerr rotation in the blue spectral region renewed scientific interest in MnBi as possible MO recording media.[13] The large magnetocrystalline anisotropy $K_1 + K_2 = 1.2\times 10^6$ J/m^3 at room temperature[14] of hexagonal MnBi leads in the case of c-axis oriented films to an out-of-plane easy magnetic axis necessary for using the polar Kerr effect as the read-out method for MO stored data.[15]

The crucial materials properties necessary for thermomagnetic writing[16] are a stable structural phase over the entire temperature range and a significantly lower coercivity at higher temperatures. However, pure MnBi undergoes a first order structural phase transition at $T = 628$ K from the ferromagnetic low temperature phase (LTP) to a paramagnetic high temperature phase (HTP) of $Mn_{1.08}Bi$.[17–19] In the LTP with the lattice constants $a_{\mathrm{LTP}} = 0.429$ nm and $c_{\mathrm{LTP}} = 0.613$ nm, the Mn atoms occupy the octahedral sites, whereas the Bi atoms fill half of the bipyramidally coordinated interstices of the NiAs-type unit cell.[20] At the phase transition from the LTP to the HTP 10%–15% of the Mn atoms shift to the unoccupied interstices, leading to slightly changed lattice constants of $a_{\mathrm{HTP}} = 0.434$ nm and $c_{\mathrm{HTP}} = 0.597$ nm.[18,21] This first-order phase transition can be understood as a peritectic phase decomposition from MnBi to $Mn_{1.08}Bi$ and pure Bi. This phase transition and especially the recrystallization from $Mn_{1.08}Bi$ back to MnBi is detrimental for the application of a thermomagnetic writing process.

Besides the structural phase transition the observed increase of the coercive field H_c with increasing temperature above room temperature also prevents the application of a thermomagnetic writing process. As shown in previous articles[14,22] the coercivity of pure MnBi continuously in-

a)Author to whom correspondence should be addressed; electronic mail: ruediger@physik.rwth-aachen.de

creases from $H_c = 0.25\,\mathrm{T}$ at room temperature to $H_c = 2.0\,\mathrm{T}$ at $T = 550\,\mathrm{K}$.

Much effort was spent stabilizing the LTP, such as decoupling the structural and the magnetic phase transition via doping MnBi with transition metal atoms. Here, two alternative approaches are possible.

By occupying the interstices with transition metal ions preferring the fivefold-coordinated bipyramidal interstices the structural phase transition to the HTP could be suppressed.[23–28] Nevertheless, clear experimental proof of the validity of this concept has not been presented in these articles.

On the other hand doping with trivalent ions, which prefer the octahedral coordination of the octahedral sites in the MnBi unit cell and substitute for the Mn atoms but favor antiferromagnetic exchange, allows a continuous decrease of the Curie temperature with increasing dopant concentration. Most recently, a clear reduction of the effective Curie temperature of ternary $Mn_{0.9}Cr_{0.1}Bi$ has been reported.[29,30] For these samples the Curie temperature is reduced to approximately 520 K, which is well below the structural phase transition temperature of $T = 628\,\mathrm{K}$.

The increase of the coercivity of pure MnBi at high temperature has been explained on the basis of a hybrid domain wall pinning model.[14] As reported before, multilayered MnBi/Al thin films or, in general, MnBi thin films with a small Al content exhibit a clear reduction of the MnBi grain size[4,22,31–33] in comparison to pure MnBi films of similar thickness without a significant change of the MO performance.[4,22,31,32] A cosputtering technique has been employed, which leads to a MnBi grain size of only 20 nm without using any dopants.[34]

In the MnBi/Al multilayered films reported the average MnBi grain size becomes smaller than approximately 50 nm and a dramatic change in the magnetization reversal process has been observed from one driven by domain wall motion toward coherent rotation. For a magnetization reversal process via coherent rotation a domain wall pinning mechanism is not relevant and, therefore, cannot govern the high temperature properties of MnBi. In this article we report on the relationship between MnBi grain size, micromagnetic properties, and the high temperature properties of multilayered MnBi/Al thin films.

II. EXPERIMENTAL METHODS

c-axis oriented MnBi/Al films have been prepared via thermal evaporation of Bi(18 nm)/Mn(12 nm)/Al(d_{Al})/Bi(18 nm)/Mn(12 nm) multilayers on quartz substrates in a vacuum of $\sim 10^{-6}$ mbar.[35] The deposition rate of Bi is critical for getting *c*-axis oriented MnBi layers and has been adjusted to only 0.04 nm/s, whereas the Mn and Al layers have been deposited at a larger rate of 0.5 nm/s.[36] All films were protected with a 2 nm thick Al capping layer. During deposition the substrate temperature was held at ambient temperature. After deposition the multilayers were annealed for 30 min at 653 K and for 30 min at 593 K in a vacuum of $\sim 10^{-5}$ mbar. During this annealing procedure the Mn atoms diffuse into the Bi layers forming *c*-axis oriented MnBi.[37,38]

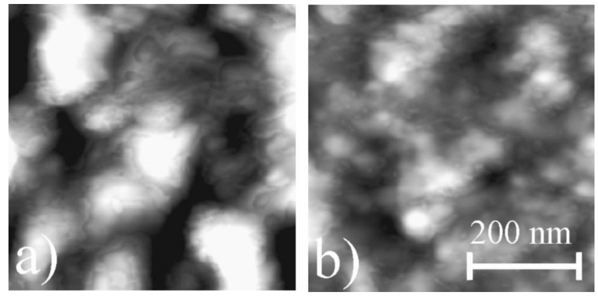

FIG. 1. AFM images of multilayered MnBi/Al films with: (a) a 0.2 nm and (b) a 2.0 nm thick Al interlayer.

The structural and magnetic properties were characterized by x-ray diffraction analysis, Rutherford backscattering (RBS), transmission electron microscopy (TEM), polar Kerr hysteresis loop measurements in a temperature range from $T = 10$ to 730 K, as well as polar Kerr spectroscopy in a photon energy range from 0.8 to 5.2 eV, and atomic and magnetic force microscopy (AFM/MFM). For the high temperature hysteresis loop measurements determining the high temperature coercivity of MnBi/Al films, the samples were mounted on a heatable copper block within a high vacuum chamber with *in situ* hysteresis loop capabilities.

III. STRUCTURAL AND MAGNETIC PROPERTIES

During annealing Mn atoms diffuse into the *c*-axis oriented Bi layers. At randomly distributed nucleation sites MnBi seeds will be formed and grow to MnBi grains.[39,40] Here, *c*-axis orientation of the resulting MnBi/Al films can be achieved only if the Bi layers show the same orientation before annealing. The *c*-axis lattice constant of the MnBi/Al films has been determined to be $c_{\mathrm{LTP}} = 0.61 \pm 0.02\,\mathrm{nm}$, which is close to the value of pure MnBi. RBS and TEM measurements reveal that the Al interlayer acts as a diffusion barrier during the alloying process and remains as a continuous interlayer between the MnBi layers and partly diffuses within the grain boundaries.[35] The stability of the Al interlayer is presumably based on partial oxidization of the Al to Al_2O_3, which has a higher thermal stability than pure Al.[41] Therefore, the alloying process takes place in each individual Bi/Mn bilayer, whereas the diffusion across the Al interlayer is suppressed. Also TEM measurements on MnBi/Al films with a 2.0 nm thick Al interlayer have confirmed the presence of a remaining Al (Al_2O_3) interlayer after annealing. The reduced interdiffusion due to the presence of Al interlayers leads to significantly smaller MnBi grain sizes compared to pure MnBi films of comparable thickness.[35] The average MnBi grain size of pure MnBi films is approximately 200 nm. Figure 1 shows AFM images of MnBi/Al films with: (a) a 0.2 nm thick and (b) a 2.0 nm thick Al interlayer. For the MnBi/Al film with a 0.2 nm thick Al interlayer the rms roughness of the film and the average MnBi grain size are 21 and 100 nm, respectively. In contrast, using a 2.0 nm thick Al interlayer both the rms roughness amplitude and the average MnBi grain size are clearly reduced to be 14 and 43 nm, respectively. Presumably the Al interlayer (which is partially oxidized) surrounds the MnBi

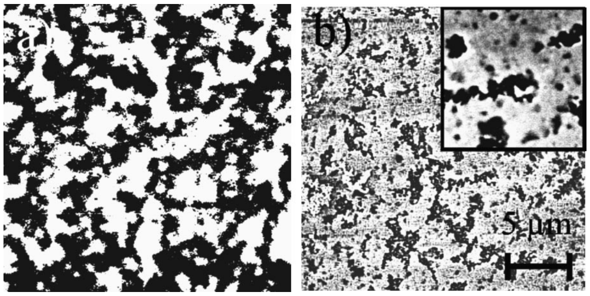

FIG. 2. MFM images of multilayered MnBi/Al films with: (a) a 0.2 nm and (b) a 2.0 nm thick Al interlayer in zero applied field after demagnetization. The size of the inset in (b) is 5 μm$\times$5 μm.

grains and is segregated at the grain boundaries, which reduces interdiffusion across grain boundaries leading to the observed reduction in MnBi particle size. Nevertheless, a local chemical analysis has not been performed.

Polar Kerr hysteresis loop measurements were performed on MnBi/Al films with 0.2, 1.4, and 2.0 nm thick Al interlayers. All films show nearly 100% remanence and an increasing coercivity as the Al interlayer thickness increases.[40] For MnBi/Al films with 0.2, 1.4, and 2.0 nm Al interlayers coercivities of 0.35, 0.75, and up to 0.85 T have been determined at room temperature (RT), respectively. This is a clear indication that the Al content has an impact on the MnBi grain size and micromagnetics.[40] Recently, the correlation between MnBi grain size and coercivity has been demonstrated via simulating the magnetization reversal process as a function of the MnBi particle size using a Monte Carlo method.[42]

Figure 2 shows MFM images of MnBi films with: (a) a 0.2 nm thick and (b) a 2.0 nm thick Al interlayer after demagnetizing the films. The CoCr MFM tips used are vertically magnetized highlighting the out-of-plane component of the magnetization. The MnBi film with a 0.2 nm thick Al interlayer exhibits magnetic domains which are approximately 1–2 μm in size. The domain size is larger than the MnBi grain size, which has been determined to be 100 nm. The volume of one magnetic domain contains 100–400 MnBi grains. Here, the magnetization reversal mechanism is dominated by nucleation of a few reversed domains which expand via domain wall movement. This leads to domain sizes which are much larger than the grain size of the system.

In contrast, for the MnBi film with a 2 nm thick Al interlayer [see Fig. 2(b)] a very small domain size in the range of a few MnBi grains has been observed, with the domain boundaries showing fractal-like symmetry. The inset shows a magnification (16$\times$) of the same domain pattern. This is a clear indication of an individual magnetization reversal process within each grain. A weaker magnetic coupling between neighboring MnBi grains due to Al or Al_2O_3 within the grain boundaries also suppresses a magnetization reversal via domain wall movement across grain boundaries. This leads to the observed significantly smaller domain size in the demagnetized state in comparison to the MnBi/Al film with a 0.2 nm thick Al interlayer.

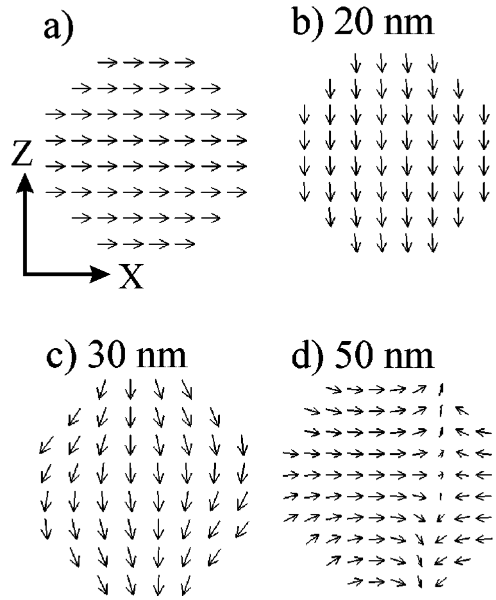

FIG. 3. Simulated size dependent magnetic spin structures of MnBi spheres during magnetization reversal: side view (x-z plane) at: (a) magnetic saturation of a 20 nm MnBi sphere, and side views (x-z plane) of (b) a 20 nm, (c) a 30 nm, and (d) a 50 nm MnBi sphere at the moment of magnetization reversal (coercive field is applied along the negative x axis).

IV. MICROMAGNETIC SIMULATIONS

In order to confirm the experimental observation of a change in the type of magnetization reversal process as a function of MnBi grain size micromagnetic simulations have been performed. For this purpose isolated MnBi grains (spheres) have been assumed and, therefore, interactions between grains via magnetic exchange and long-range dipole–dipole interaction have been neglected. Neglecting the magnetic exchange between MnBi grains is only valid if the grain boundaries are assumed to be nonmagnetic and thicker than 3 nm. For the MnBi/Al film with a 2.0 nm thick Al interlayer the amount of Al (Al_2O_3) within the MnBi grain boundaries is large enough to suppress a domain wall motion, which justifies the assumption of isolated MnBi grains for the simulation of the magnetization reversal process.

The magnetic domain patterns during magnetization reversal of isolated MnBi spheres with diameters of 20, 30, and 50 nm have been computed with the Landau–Lifshitz–Gilbert (LLG) Micromagnetics Simulator.[43] The equilibrium magnetization was found by solving the LLG equation.[44] In this equation, the effective field acting on the spins is determined from the total energy of the system, which incorporates the effect of magnetic exchange energy ($A=1.2\times10^{-11}$ J/m), magnetocrystalline uniaxial anisotropy ($K_u=K_1+K_2=1.2\times10^6$ J/m^3), magnetostatic energy ($M_s=660$ kA/m), and the Zeeman term.[42] The continuous magnetization distribution was approximated by a discrete cubic mesh, with a cell volume of 8–16 nm^3.

Figure 3 shows the x-z plane of the simulated magnetic domain configurations at: (a) magnetic saturation (parallel to the positive x axis) for a 20 nm MnBi sphere and at the coercive field for a: (b) 20 nm, (c) 30 nm, and (d) 50 nm MnBi particle. For the simulation the uniaxial anisotropy of

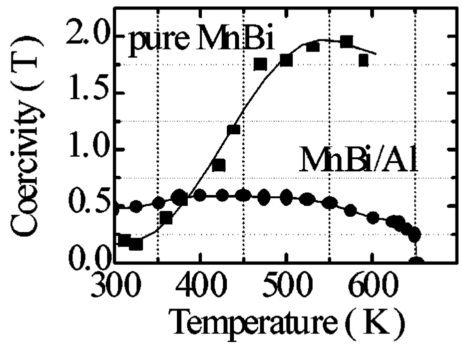

FIG. 4. High temperature coercivity of a pure MnBi film (solid rectangles; data taken from Ref. 14) and a multilayered MnBi/Al film with a 2.0 nm thick Al interlayer (solid circles).

the particles has been set parallel to the *x* axis [see Fig. 3(a)]. The applied magnetic field (coercive field) in Figs. 3(b)–3(d) is aligned parallel to the negative *x* axis. The arrows indicate the magnetization direction within the discretized mesh cells of the particle. For the 20 nm MnBi particle [Fig. 3(b)] the magnetization reversal purely occurs via coherent rotation, whereas for the 30 nm particle [Fig. 3(c)] not all cells rotate in-phase, but rather a buckling of the magnetization near the boundary arises. The 50 nm MnBi particle in Fig. 3(d) finally shows a reversal process dominated by domain wall movement.

For all particle diameters the calculated coercivity varies in the range of 3 T, which is close to the theoretical limit of $H_c = 2K_u/M_s = 3.5\,\mathrm{T}$. The large difference between the experimental value for a MnBi/Al film with a 2 nm thick Al interlayer at RT and the theoretical one has a number of possible origins. First, the calculation has been performed at $T = 0\,\mathrm{K}$. Thermal fluctuations at room temperature lead to a significant reduction of the theoretical limit. Furthermore, misalignment from a strict *c*-axis orientation of individual MnBi grains, size, and shape variations of MnBi grains, long-range dipolar interactions, and the presence of exchange interactions between neighboring MnBi grains, induce a reduction of the experimental coercivity in comparison to the theoretical limit.

V. HIGH TEMPERATURE COERCIVITY

Figure 4 shows the temperature dependence of the coercivity from RT to 650 K of a pure MnBi film (data taken from Ref. 14) in comparison with a MnBi/Al film with a 2.0 nm thick Al interlayer. For pure MnBi films the high temperature coercivity increases from 0.2 T at RT to approximately 2.0 T in the range of 550 K. In contrast, the MnBi/Al film exhibits at RT a slightly higher coercivity of 0.5 T but only a moderate increase to 0.6 T between 400 and 500 K. For higher temperatures the coercivity decreases continuously until at $T = 650\,\mathrm{K}$ the phase transition from the LTP to the HTP occurs where the coercivity rapidly drops to zero. The suppression of the dramatic increase of the high temperature coercivity for the multilayered MnBi/Al film is directly related to the magnetization reversal mechanism via coherent rotation observed for MnBi/Al films with a 2.0 nm thick Al interlayer. During the coherent magnetization reversal no domain wall nucleates and, therefore, domain wall pinning is not the dominant mechanism.

In the present form the interpretation of the suppression of the high temperature coercivity on the basis of a coherent magnetization reversal process is not consistent with an observation[4] made on the quenched HTP of MnBi,[19,45] where unoccupied interstices are partially filled with Mn atoms. In this article the high temperature coercivity has been correlated with an increasing fraction of the quenched HTP for increasing quenching temperatures. The authors suggest that the change in structure at higher temperatures, i.e., partially filled interstices, is the origin of the rapid increase of the high temperature coercivity of the LTP. Nevertheless, this conclusion contradicts the observed high temperature coercivity of pure MnBi, which shows a rapid increase of the coercivity with a maximum of up to $H_c = 1.9\,\mathrm{T}$ at $T = 550\,\mathrm{K}$ (see Fig. 4).[6,14] Following the arguments above, the occupation of the interstices with Mn atoms has to be a continuous process being also present at more than 200 K below the structural phase transition temperature of 628 K from the LTP to the HTP which is highly unlikely.

VI. SUMMARY

During the MnBi formation process Al interlayers suppress the interdiffusion between individual MnBi layers, which leads to a MnBi grain size in the range of 40 nm. The smaller MnBi grain size has been correlated with the change of the magnetization reversal process from one driven by domain wall movement toward one dominated by coherent rotation. This results in MnBi/Al multilayers to the observed suppression of the increase in coercivity at higher temperature. Micromagnetic calculations reveal such a change of the magnetization reversal process for MnBi particle diameters between 30 and 50 nm, which is consistent with the observed MnBi grain size.

ACKNOWLEDGMENT

This work was supported by the German Federal Ministery for Education and Research ‘‘BMBF’’ under Grant No. 13N6178/2.

[1] H. J. Williams, R. C. Sherwood, F. G. Foster, and M. Kelly, J. Appl. Phys. **28**, 1181 (1957).
[2] B. W. Roberts and C. P. Bean, Phys. Rev. **96**, 1494 (1954).
[3] D. Chen, J. F. Ready, and E. Bernal, J. Appl. Phys. **39**, 3916 (1968).
[4] D. J. Sellmyer, R. D. Kirby, J. Chen, K. W. Wierman, J. X. Shen, Y. Liu, B. W. Robertson, and S. S. Jaswal, J. Phys. Chem. Solids **56**, 1549 (1995).
[5] G. Q. Di, S. Iwata, and S. Uchiyama, J. Magn. Magn. Mater. **104–107**, 1023 (1992).
[6] U. Rüdiger, J. Köhler, A. D. Kent, T. Legero, J. Kübler, P. Fumagalli, and G. Güntherodt, J. Magn. Magn. Mater. **198–199**, 261 (1999).
[7] T. Suzuki, MRS Bull. **9**, 42 (1996).
[8] J. Köhler and J. Kübler, J. Phys.: Condens. Matter **8**, 8681 (1996).
[9] R. F. Sabiryanov and S. S. Jaswal, Phys. Rev. B **53**, 313 (1996).
[10] S. S. Jaswal, J. X. Shen, R. D. Kirby, and D. J. Sellmyer, J. Appl. Phys. **75**, 6346 (1994).
[11] K. U. Harder, D. Menzel, T. Widmer, and J. Schoenes, J. Appl. Phys. **84**, 3625 (1998).
[12] P. M. Oppeneer, V. N. Antonov, T. Kraft, H. Eschrig, A. N. Yaresko, and A. Y. Perlov, J. Appl. Phys. **80**, 1099 (1996).
[13] G. Fasol, Phys. Bl. **52**, 101 (1996).

[14] X. Guo, X. Chen, Z. Altounian, and J. O. Ström-Olsen, J. Appl. Phys. **73**, 6275 (1993).
[15] J. Kerr, Philos. Mag. **3**, 321 (1877).
[16] C. D. Mee and E. D. Daniel, *Magnetic Recording Volume I+II: Computer Data Storage* (Mc Graw–Hill, New York, 1988).
[17] A. U. Seybold, H. Hansen, B. W. Roberts, and P. Yurcisin, J. Met. **8**, 616 (1956).
[18] T. Chen and W. E. Stutius, IEEE Trans. Magn. **MAG-10**, 581 (1974).
[19] T. Chen, J. Appl. Phys. **45**, 2358 (1974).
[20] N. Henry and K. Londsdale, *International Tables of X-Ray Crystallography* (Kynoch, Oxford, 1952).
[21] A. F. Andresen, J. E. Engebresten, and J. Refsnes, Acta Chem. Scand. **26**, 175 (1972).
[22] U. Rüdiger, T. Roos, G. Güntherodt, B. Holländer, and P. Fumagalli, Appl. Phys. Lett. **70**, 2604 (1997).
[23] E. Feldkeller, IEEE Trans. Magn. **MAG-8**, 481 (1972).
[24] W. K. Unger, E. Wolfgang, H. Harms, and H. Haudek, J. Appl. Phys. **43**, 2875 (1972).
[25] W. K. Unger, Phys. Status Solidi A **13**, 527 (1972).
[26] S. Yoshii and K. Egashira, IEEE Trans. Magn. **MAG-10**, 587 (1974).
[27] H. Göbel, E. Wolfgang, and H. Harms, Phys. Status Solidi A **34**, 553 (1976).
[28] H. Göbel, E. Wolfgang, and H. Harms, Phys. Status Solidi A **35**, 89 (1976).
[29] P. R. Bandaru, T. D. Sands, Y. Kubota, and E. E. Marinero, Appl. Phys. Lett. **72**, 2337 (1998).
[30] P. R. Bandaru, T. D. Sands, D. Weller, and E. E. Marinero, J. Appl. Phys. **86**, 1596 (1999).
[31] J. X. Shen, R. D. Kirby, D. J. Sellmyer, and Y. J. Wang, J. Appl. Phys. **69**, 5984 (1991).
[32] K. W. Wierman, J. X. Shen, R. D. Kirby, and D. J. Sellmyer, J. Appl. Phys. **75**, 6348 (1994).
[33] Y. J. Wang, C. P. Luo, L. C. Kong, X. S. Xi, D. Huang, and Y. Chen, J. Magn. Soc. Jpn. **17**, 294 (1993).
[34] J. Chen, R. D. Kirby, and D. J. Sellmyer (unpublished).
[35] U. Rüdiger, P. Fumagalli, H. Berndt, A. Schirmeisen, B. Holländer, and G. Güntherodt, J. Appl. Phys. **80**, 196 (1996).
[36] M. Nakada and M. Okada, IEEE Trans. Magn. **30**, 4431 (1994).
[37] S. Honda and T. Kusuda, Appl. Phys. **45**, 2689 (1974).
[38] M. A. Angadi and V. Thanigaimani, J. Mater. Sci. Lett. **10**, 285 (1991).
[39] L. Mayer, J. Appl. Phys. **31**, 384S (1960).
[40] U. Rüdiger, H. Berndt, A. Schirmeisen, P. Fumagalli, and G. Güntherodt, J. Appl. Phys. **78**, 5391 (1995).
[41] P. Fumagalli, U. Rüdiger, P. Dworak, B. Holländer, U. Nowak, and G. Güntherodt, J. Magn. Soc. Jpn. **20-S1**, 433 (1996).
[42] U. Nowak, U. Rüdiger, P. Fumagalli, and G. Güntherodt, Phys. Rev. B **54**, 13017 (1996).
[43] LLG Micromagnetics Simulator is a commercially available micromagnetics code written by Michael Scheinfein. More informations can be found on the Web site: www.dancris.com\~llg; Some details on the numerical methods can be found in M. R. Scheinfein *et al.*, Phys. Rev. B **43**, 3395 (1991).
[44] A. Aharoni, *Introduction to the Theory of Ferromagnetism* (Clarendon, Oxford, 1996).
[45] A. F. Andresen, W. Hälg, P. Fischer, and E. Stoll, Acta Chem. Scand. **21**, 1543 (1967).